Investigation of new narrow-bandwidth *a*-Si : H photodetector

N.-F. Shin
J.-W. Hong
Y.-F. Wu
T.-S. Jen
C.-Y. Chang

Indexing terms: Amorphous silicon, Photodetectors

Abstract: A narrow-bandwidth hydrogenated amorphous silicon (*a*-Si : H) photodetector with a basic structure of Al/n^+-i-p^+-i-n-i-p-i-n^+/ITO/glass has been investigated. The spectral response of this new photodetector was found to be affected by the absorption coefficient of *a*-Si : H material, surface recombination current, device layer thicknesses, and applied bias. The spectral response of this device reveals a measured minimum FWHM of 58 nm at zero volt bias. The peak wavelength in the visible spectrum can be shifted from 400 nm (purple) to 550 nm (green) by decreasing the bias voltage from 5 to 0 V. The optoelectronic characteristics of this photodetector fit theoretically using suitable quantitative estimates.

1 Introduction

Hydrogenated amorphous silicon (*a*-Si : H) has been widely used in the fabrication of photosensitive devices, such as solar cells [1, 2], photoreceptors for electrophotography [3], vidicons [4], and integrated contact image sensors for facsimile or optical character recognition [5]. In 1986, the first heterojunction Al/n^+(*a*-Si : H)/n-i-p(*a*-SiC : H)/i-n^+(*a*-Si : H)/ITO phototransistor with high gain ($\sim$40) and high speed ($\sim$10 μs) was developed by C. Y. Chang *et al.* [6, 7]. The spectral response of this device contains a voltage-dependent peak wavelength of between 400 to 630 nm (violet to red) with a typical FWHM (full width at half max.) of 200 nm. In 1987 and 1988, a two-colour Al/n(*a*-SiC : H)/i-p(*a*-Si : H)/i-n(*a*-SiC : H)/ITO detector and a three-colour Al/n-i-i-p(*a*-Si : H heterojunction)/i(*a*-SiC : H)/i(*a*-Si : H)/n(*a*-SiC : H)/ITO detector were developed sequentially by S. C. Lee *et al.* [8, 9]. The two-colour detector has good response ratios for 450 nm (purple) and 600 nm (orange) light. The three-colour detector, with a typical FWHM greater than 100 nm, has peak responses at 480 nm (blue), 530 nm (green), and 575 nm (green) light at applied voltages of 2, -0.2, and -2 V, respectively, and therefore can be used to sense blue, green, and orange or red light. In 1991, a glass/ITO/*a*-Si : H/Cr photodiode with a voltage-selectable spectral response was developed by Y.K. Fang *et al.* [10]. This diode consists of two back-to-back Schottky junctions and has peak responses of 480 nm (blue), 530 nm (green), and 620 nm (orange) at 0.5, 1.5, and -1.5 V applied biases, respectively. Although the spectral responses of the above-mentioned photosensitive devices depend on device structure as well as applied bias, these amorphous photodetectors have disadvantages, such as limited peak-wavelength range of voltage-selectable spectral response, wide FWHM, and higher subpeak spectral response. In this paper, we propose to use a new homojunction *a*-Si : H amorphous photodetector with a basic structure of Al/n^+-i-p^+-i-n-i-p-i-n^+/ITO/glass. We have investigated photodetector characteristics, both experimentally and theoretically to reduce the FWHM. Compared with the Al/n^+-i-p^+-i-n^+/ITO/glass *a*-Si : H phototransistor, which does not have a voltage-selectable spectral response [11], the additional thin n-i-p-i layers are included in the proposed photodetector to modify the shape of spectral response and enhance the spectral response in the middle- and short-wavelength ranges of visible spectrum. It is thought that the additional layers may modify the internal electric-field profile of the photosensitive device.

2 Device fabrication

We used ITO-coated Corning 7059 glass substrates which after cleaning were put into the chamber of ULVAC model CPD-1108D plasma-enhanced chemical vapour deposition system. The reaction chamber was pumped down to 3.9×10^{-6} torr and heat-cleaned by a substrate heater at 250°C for 90 min. sequentially. Then, the $n^+(d_n^+)$, $i(d_4)$, $p(d_p)$, $i(d_3)$, $n(d_n)$, $i(d_2)$, p^+, $i(d_1)$, and n^+ *a*-Si : H layers (with thicknesses as indicated in Fig. 1 and lower part of Table 1 for devices 1 and 2) were deposited in succession. The collector thickness of the proposed device, which is equal to $d_2 + d_n + d_3 + d_p + d_4 + d_n^+$, was kept around 300 nm to ensure nearly total absorption of incident light [11]. The n^+ (or n) layers were

Paper 9800J (E3), first received 18th January and in revised form 14th June 1993

N.-F. Shin, J.-W. Hong, Y.-F. Wu and T.-S. Jen are with the Department of Electrical Engineering, National Central University, Chungli, Taiwan, 32054, Republic of China

C.-Y. Chang is with the Institute of Electronics, National Chiao Tung University, Hsinchu, Taiwan, 30050, Republic of China

This work was supported by National Science Council, Republic of China, under contract NSC 78-0417-E008-02

Table 1: Parameters and device layer thicknesses used in I_{sa} and $\Delta\phi_t$ calculations

Parameters	Sample		Description
	1	2	
A (m²)	1.13×10^{-6}	1.13×10^{-6}	Device area
A^* (A/K² cm²)	550.8	550.8	Richardson's constant
T (K)	300	300	Operating temperature
R	0.2	0.2	Reflection coefficient
C	5×10^{-22}	6.7×10^{-22}	Proportionality constant
τ_{eff} (s)	1×10^{-6}	2.9×10^{-6}	Effective hole lifetime
x_j (nm)	30	20	$d_n^+ + d_4$
L_p (μm)	36.9	36.9	Hole diffusion length
D_p (m²/s)	9×10^{-5}	9×10^{-5}	Hole diffusion constant
S_p (m/s)	1000	1000	Surface recombination velocity
I_{ps} (A)	1.59×10^{-20}	28.8×10^{-20}	Hole saturation current
η	6.85	6.51	Diode ideality factor[1]
n	1.11	1.01	Diode ideality factor[2]
d_1	20	20	Device layer thickness as indicated in Fig. 1
d_2	240	240	
d_n	20	10	
d_3 nm	20	15	
d_p	20	10	
d_4	20	10	
d_n	10	10	

1 Accounts for hopping of carriers along gap state of *a*-Si : H
2 Accounts for saturation effect at high collector current under high incident light power

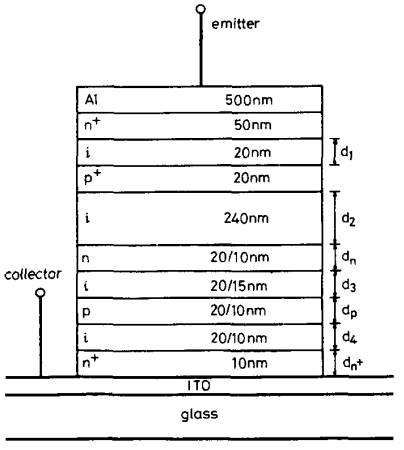

Fig. 1 *Schematic cross-section of a-Si : H photodetector*

deposited by introducing diluted silane (96% H_2 + 4% SiH_4) and phosphine (99% H_2 + 1% PH_3) kept at a flow-rate ratio of 25 : 8 (or 25 : 2) into the reaction chamber. The i layers were deposited by introducing only the diluted silane into the reaction chamber. The p^+ (or p) layers were deposited by introducing the diluted silane and diborane (99% H_2 + 1% B_2H_6) keeping a flow-rate ratio of 25 : 4 (or 25 : 1) into the reaction chamber. The substrate temperature, gas pressure, and RF power density were kept at 250°C, 0.3 torr, and 0.16 W/cm², respectively, during the depositions of various films. To avoid the i-layer contamination caused by the dopant gases outgassing from the reaction chamber and the pipes, the system was purged by H_2 and evacuated after the deposition of each doped layer. Finally, a 500 nm Al layer was thermally evaporated through a metal mask to form a circular emitter electrode. The device area $A = 1.13 \times 10^{-2}$ cm².

3 Theoretical analysis

Fig. 2 shows the schematic optical bandgap diagrams of the proposed device under equilibrium, and normal operation ($V_{CE} > 0$) with incident light illuminating on the substrate side. Assuming full depletion, all of the *a*-Si : H device layers are completely depleted of free carriers at any bias condition if there is no incident light. Under normal operation with incident light, the incident photons generate electron–hole pairs mainly in the reverse-biased, thicker, and undoped d_2 and d_4 regions. The photogenerated holes in d_2 (or d_4) region drift upward to the first (or second) hole potential valley, and are partially accumulated in the valley. Also, the photogenerated electrons in d_2 region are partially accumulated in the electron potential valley between the first and

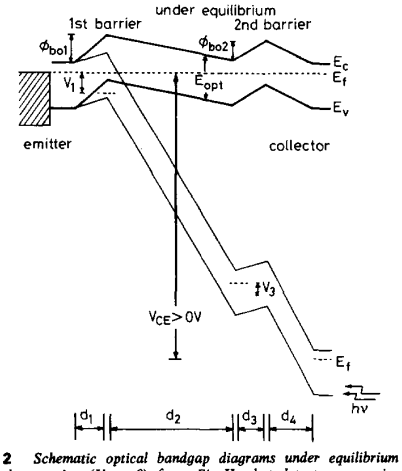

Fig. 2 *Schematic optical bandgap diagrams under equilibrium and normal operation ($V_{CE} > 0$) for a-Si : H photodetector, assuming full depletion*

– – – – Fermi levels
Optical bandgap E_{opt} = 1.76 eV for *a*-Si : H

second potential barriers, after drifting down the first electron potential barrier. These accumulated holes and electrons induce further a barrier lowering $\Delta\phi_{l1}$ (or $\Delta\phi_{l2}$) at the first (or second) potential barrier, which in turn enhances the electron and hole currents. The total device barrier lowering due to accumulated carriers $\Delta\phi_l = \Delta\phi_{l1} + \Delta\phi_{l2}$ under normal operation ($V_{CE} > 0$).

At high bias ($V_{CE} > 15$ V for device 1, and > 10 V for device 2), we assume the holes may inject into the emitter from the first hole potential valley and the electrons may inject into the d_4 layer from the electron potential valley directly. This assumption is reasonable in consideration of the higher kinetic energy of these carriers owing to $d_2 \gg d_4$ and the barrier lowerings caused by the applied V_{CE} bias and the accumulated carriers. The hole current I_{pl}^H injected into the emitter could be expressed as [12, 14]

$$O_{pl}^H = I_{ps} e^{\Delta\phi_l^H/nkT}(e^{qV_3/\eta kT} - 1) \quad (1a)$$

and the electron current I_{nl2}^H collected by the collector could be expressed as [12, 14]

$$I_{nl2}^H = AA^*T^2 e^{-q(\phi_{bo} - \Delta\phi_l^H)/nkT}(e^{qV_1/\eta kT} - 1) \quad (1b)$$

where A^* is the effective Richardson's constant, ϕ_{bo} ($= \phi_{bo1} + \phi_{bo2}$ in Fig. 1) the total potential barrier height under equilibrium, I_{ps} the hole saturation current, $\Delta\phi_l^H$ the total barrier lowering due to accumulated carriers at high V_{CE} bias, n the diode ideality factor which accounts for the saturation effect at high collector-current level under high incident light power, η the ideality factor which accounts for the hopping of carriers along the gap state of a-Si : H, $V_1 \simeq d_1 V_{CE}/d$ and $V_3 \simeq (d_3 V_{CE})/d$ the first and second potential barrier lowerings due to applied V_{CE} voltage under fully depleted and δ-doped assumptions, and $d \simeq d_1 + d_2 + d_3 + d_4$ the total i-layer thickness of the device [11, 13, 15]. At low bias ($V_{CE} < 7$ V for device 1 and < 3 V for device 2), the hole current I_{pl}^L injected into the emitter is [12, 14]

$$I_{pl}^L = I_{ps} e^{\Delta\phi_l^L/nkT}(e^{qV_3/\eta kT} - 1)(e^{qV_1/\eta kT} - 1) \quad (1c)$$

and the electron current I_{nl2}^L collected by the collector is [12, 14]

$$I_{nl2}^L = AA^*T^2 e^{-q(\phi_{bo} - \Delta\phi_l^L)/nkT} \times (e^{qV_1/\eta kT} - 1)(e^{qV_3}/\eta kT - 1) \quad (1d)$$

where $\Delta\phi_l^L$ the total barrier lowering due to accumulated carriers at low V_{CE} bias. The collector photocurrent, which is equal to the sum of the electron current and the negligible hole current, can be approximated by I_{nl2}^H or I_{nl2}^L described in eqn. 1b or 1d. The corresponding collector dark current I_{nd2}^H or I_{nd2}^L can be obtained by putting $\Delta\phi_l^H$ or $\Delta\phi_l^L = 0$.

By analogy of the analysis for a single bulk-barrier phototransistor [12], the principle of detailed balance for holes can be used to obtain $\Delta\phi_l$. The generated hole flux Φ_l which recombines at a negligible rate of I_{rc} in the d_2 and d_4 regions and at a rate of surface recombination current I_{SR} at ITO–n^+ collector interface, is balanced by the hole current I_{pl} injected into the emitter, and the hole recombination current I_{RB} owing to traps in the two p-type regions. By neglecting recombination currents in all regions except I_{RB}, the rate equation can be expressed as [12, 13]

$$A\Phi_l = I_{pl} + I_{RB} + I_{SR} \quad (2)$$

where $I_{RB} = (C/\tau_{eff})e^{\Delta\phi_l/nkT}$ in which C is the proportionality constant and τ_{eff} is the effective hole lifetime [13]. Using eqns. 1a and 2, $\Delta\phi_l$ at high V_{CE} bias ($\Delta\phi_l^H$) can be obtained by putting $I_{pl} = I_{pl}^H$, i.e.

$$\Delta\phi_l^H = \frac{nkT}{q} \ln\left(\frac{A\Phi_l - I_{SR}}{I_{ps} e^{qV_3/\eta kT} + C/\tau_{eff}}\right) \quad (3a)$$

Similarly, using eqns. 1b and 2, $\Delta\phi_l$ at low V_{CE} bias ($\Delta\phi_l^L$) can be obtained by putting $I_{pl} = I_{pl}^L$, and

$$\Delta\phi_l^L = \frac{nkT}{q} \ln\left(\frac{A\Phi_l - I_{SR}}{I_{ps}(e^{qV_3/\eta kT} - 1)(e^{qV_1/\eta kT} - 1) + C/\tau_{eff}}\right) \quad (3b)$$

As can be seen from the logarithmic dependence of eqn. 3a or 3b, the gradual saturation of $\Delta\phi_l^H$ or $\Delta\phi_l^L$ at high incident light power and high applied V_{CE} bias is to be expected because it is a requirement that the photo-induced barrier lowerings $\Delta\phi_{l1}$ and $\Delta\phi_{l2}$ must be smaller than the equilibrium barrier heights ϕ_{bo1} and ϕ_{bo2}, respectively.

The surface recombination current I_{SR} can be calculated by solving the continuity equation based on the elementary model of the p-i-n diode with two boundary conditions [16]. At the ITO–n^+ collector interface, the surface recombination current is equal to the hole current caused by diffusion from regions of high to low charge and by drift due to the influence of the electric field. At i(d_4)–p(d_p) interface, the amount of excess minority carriers (holes) is zero because this interface acts as a perfect sink for excess minority carriers (holes). I_{SR} can be expressed as [16]

$$I_{SR} = \frac{\tau_{pp} S_p \alpha[\eta_i(1-R)P_i/h\nu]}{b_p^2 - 1} \times \left\{\exp\left[\left(\frac{1}{L_{pp}} - (\alpha + E_{pp})\right)x_j\right] - 1 - \frac{\sinh(x_j/L_{pp})}{\cosh(x_j/L_{pp}) + c_p \sinh(x_j/L_{pp})} \times \left[(1 + c_p)\exp\left[\left(\frac{1}{L_{pp}} - (\alpha + E_{pp})\right)x_j\right] - (b_p + c_p)\right]\right\} \quad (4)$$

where $L_{pp} = (E_{pp}^2 + L_p)^{-1/2}$ the effective diffusion length, L_p the hole diffusion length, $\tau_{pp} = L_{pp}^2/D_p$, $b_p = L_{pp}(\alpha + E_{pp})$, $c_p = L_{pp}((S_p/D_p) + E_{pp})$, $E_{pp} = V_{CE}/2\,dkT$ the normalised electric field in the i(d_4)-type region, D_p the hole diffusion constant, S_p the surface recombination velocity, α the absorption coefficient, P_i the incident light lower, η_i the internal quantum efficiency, $h\nu$ the incident photon energy, x_j ($= d_n^+ + d_4$) the thickness between the ITO–n^+ collector interface and the i(d_4)–p(d_p) interface, and R the reflection coefficient of the illuminated surface.

4 Experimental and calculated results

The total barrier height ϕ_{bo} and the effective Richardson's constant A^* of the device can be obtained from eqn. 1b by using activation energy measurement at a high V_{CE} bias and under the dark ($\Delta\phi_l^H = 0$, $I_{nl2}^H = I_{nd2}^H$) condition. The slope of a plot of $\ln(I_{nd2}^H/T^2)$ against $1/T$ yields the total barrier height ϕ_{bo}, and its ordinate intercept at $1/T = 0$ yields the product of the device area A and the effective Richardson's constant A^* for a known high V_{CE}. The effective Richardson's constant obtained is 550.8 A/K^2 cm^2 and the total barrier height ϕ_{bo} is around 1.0 V.

Using the parameters tabulated in Table 1, Fig. 3*a* and 3*b* illustrate the calculated surface recombination current I_{SR} against V_{CE} bias voltage for device 1 and 2 under

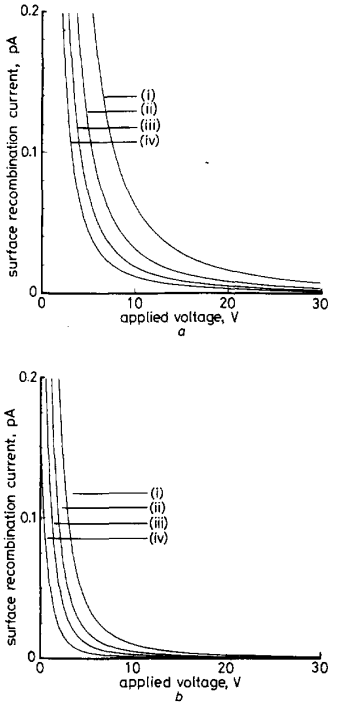

Fig. 3 *Calculated surface recombination current I_{SR} against V_{CE} bias voltage under various incident He–Ne laser powers*

(i) 0.22 mW
(ii) 0.11 mW
(iii) 65.8 μW
(iv) 41 μW
} He–Ne laser power

a Device 1
b Device 2

various incident He–Ne laser powers. The surface recombination currents for devices 1 and 2 are very similar except that the device 1 shows a much higher surface recombination current due to its thicker d_4 layer. The surface recombination current increases with the incident light power and decreases rapidly to a saturation value as the applied V_{CE} bias goes beyond 7 V for device 1 or 3 V for device 2.

Figs. 4*a* and 4*b* show the calculated total barrier lowering $\Delta\phi_t$ against bias voltage V_{CE} for devices 1 and 2 under various incident He–Ne laser powers. The calculation of the total barrier lowering $\Delta\phi_t$ was based on eqns. 3*a* and 3*b*. The total barrier lowering is very small when the applied V_{CE} bias is smaller than 3 V. It is ascribed to the larger surface recombination current when $V_{CE} < 3$ V. As the applied V_{CE} bias gradually increases beyond 3 V, the total barrier lowering increases very rapidly to a high plateau and then starts to decrease when the applied V_{CE} bias is beyond a certain voltage. When $V_{CE} > 23$ V for device 1 or > 14 V for device 2 under $P_i = 41$ μW, the decrease of the total barrier lowering is caused by the increase of hole current injected into the emitter at high bias voltage.

The photo *I–V* characteristics of the device were measured by illuminating the collector side of the device with the light emitted from a He–Ne laser. The photo *I–V*

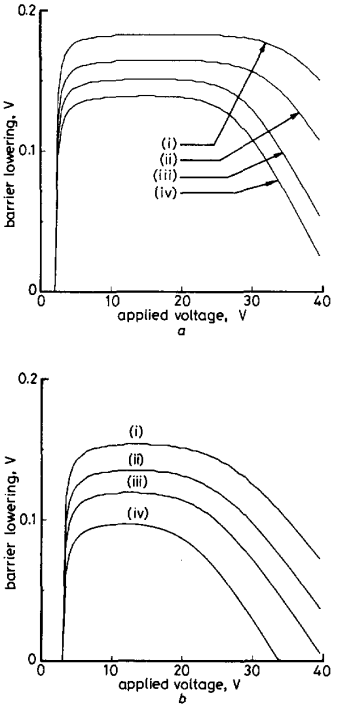

Fig. 4 *Calculated total barrier lowering $\Delta\phi_t$ due to accumulated carriers against V_{CE} bias voltage under various incident He–Ne laser powers*

(i)–(iv) laser power levels as Fig. 3
a Device 1
b Device 2

curves under various incident laser powers are shown in Fig. 5*a* for device 1 and Fig. 5*b* for device 2. The device optical gain $G = [(I_{PH} - I_d)/q]/(P_i/h\nu)$, where I_{PH} and I_d are the measured collector photo and dark currents, respectively, and can be obtained from the photo *I–V* curves. The optical gain G is dependent on the applied V_{CE} bias and the incident light power. The maximum obtainable G is 2.7 and 2.1, respectively, for device 1 at $V_{CE} = 34$ V and device 2 at $V_{CE} = 31$ V, both under $P_i = 5$ μW. From the high-V_{CE} portion of the photo *I–V* curves, the values of the total barrier lowering $\Delta\phi_t^H$ under various incident laser powers can be obtained by using eqn. 1*b*, and assuming its diode ideality factor $n = 1$. Fig. 6 gives $\Delta\phi_t^H$ against incident laser power P_i at 24°C for devices 1 and 2. From the slopes of the straight lines indicated in Fig. 6 and by using eqn. 3*a*, the diode ideality factor n obtained is 1.01 for 2 and is 1.11 for 1 [14]. These factors are close to the assumed $n = 1$ in eqn. 1*b*. The slight deviations of the factor from the ideal $n(=1)$ could be due to the influence of surface recombination current I_{SR}. (I_{SR} was assumed to be negligible in the calculation of the obtained diode ideality factor.) Device 2 has a barrier lowering slightly less than the corresponding straight-line value in the lower range of the incident laser power. This is ascribed to the prominent recom-

bination current I_{RB} in its two p-type regions. The similar phenomenon observed in the higher range of incident laser power is primarily due to the saturation of collector photocurrent at high incident laser power.

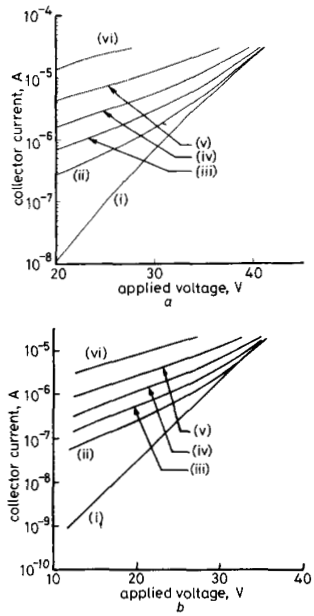

Fig. 5 *Photo I–V curves*
(i) 0 W (iv) 127 μW
(ii) 11.5 μW (v) 410 μW
(iii) 41 μW (vi) 1.8 mW
a Device 1
b Device 2

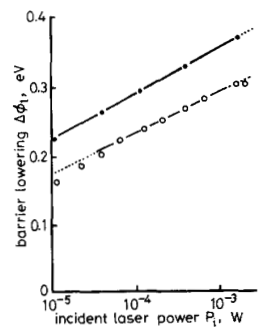

Fig. 6 *Total barrier lowering $\Delta\phi_1^n$ against input He–Ne laser power P_1*
● device 1
○ device 2

The spectral response of this proposed device could be attributed to the combined effect of the surface recombination current I_{SR}, the applied V_{CE} bias, the absorption coefficient α of the *a*-Si : H, and the device layer thicknesses. The absorption coefficient α of the fabricated *a*-Si : H film increases with increasing incident photon energy [14]. Fig. 7 describes the calculated surface recombination current I_{SR} against incident photon wavelength for device 1 with applied V_{CE} bias as a parameter.

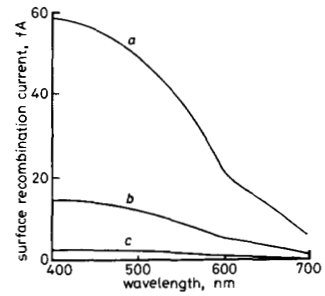

Fig. 7 *Calculated surface recombination current I_{SR} against incident photon wavelength with $P_1(\lambda) = 2$ μW for different applied V_{CE} (device 1)*
a 0 V
b 1 V
c 3 V

The surface recombination current I_{SR} decreases with increasing incident photon wavelength and increasing V_{CE} bias. The visible light having a shorter wavelength is absorbed mostly within a few hundred angstroms from the incident surface of the *a*-Si : H film. Therefore the spectral response in the shorter wavelength range can be suppressed by introducing an additional thin potential barrier near the incident surface, such as the second potential barrier of this proposed device, to increase the surface recombination current and produce a narrower FWHM.

Fig. 8 shows the calculated and experimental results of the relative spectral responses for device 1 in low V_{CE} bias

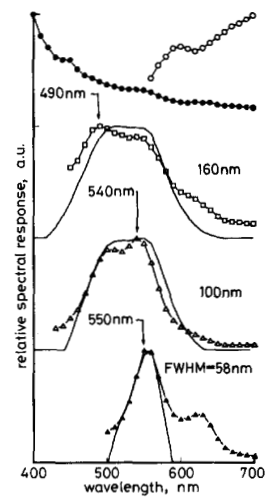

Fig. 8 *Calculated and measured relative spectral responses for device 1 under various V_{CE} biases based on incident light power $P_1(\lambda) = 2$ μW*
○ −5 V
▲ 0 V
△ 1 V
□ 3 V
● 5 V
—— Calculated

range. The incident power $P_i(\lambda) = 2\ \mu W$ at each wavelength λ. The wavelength dependence of the device photocurrent I_{PH} was measured by illuminating the collector side of the device with focused light emitted from a tungsten lamp through a monochromator. The spectral response was obtained by dividing $(I_{PH} - I_d)$ by $P_i(\lambda)/hv$. The relative spectral response was obtained after a normalisation procedure referred to the peak response value [17]. Increasing $P_i(\lambda)$ causes a slight red shift of spectral response at the same V_{CE} bias. As indicated by the experimental results, when the applied V_{CE} voltage increases from 0 to 5 V, the peak wavelength shifts from 550 nm (green) at 0 V, to 540 nm (green) at 1 V, to 490 nm (blue) at 3 V, and then towards the short-wavelength detectable limit of the measurement setup ($\simeq$400 nm) at 5 V. The FWHM $\simeq$ 58 nm at $V_{CE} = 0$ V, $\simeq$100 nm at $V_{CE} = 1$ V, and $\simeq$160 nm at $V_{CE} = 3$ V as indicated also in Fig. 9. As

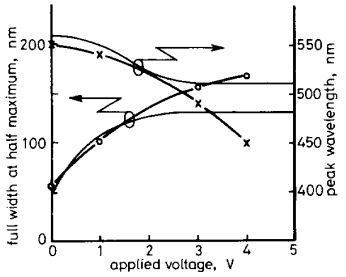

Fig. 9 *Peak wavelength and FWHM of spectral response for device 1 as function of bias voltage*
Symbols indicate experimental results

the applied V_{CE} bias increases, the responses at shorter wavelength are greatly enhanced, primarily owing to the suppression of surface recombination current I_{SR} when V_{CE} is increased. Also, there is no evident subpeak in the spectral responses. Changing the applied bias to -5 V, the peak response wavelength shifts towards the long-wavelength detectable limit of the measurement setup ($\simeq$700 nm). This phenomenon is ascribed to the longer-wavelength incident light penetrating deeply into the device d_1 and d_3 layers, which are reverse biased by the negative applied V_{CE}. The absorption edge of the *a*-Si : H used is 0.7 μm (red) [14]. The applied positive V_{CE} causes a blue shift of the spectral response. So proposed device 1 can distinguish light in the middle of the visible spectrum. The behaviour of device 2 is similar to that of a single bulk-barrier phototransistor [11]. Its spectral response is not sensitive to the increase of applied V_{CE} and peaks at a wavelength around 490 nm. Device 2 has thinner d_n, d_3, d_p and d_4 layers compared with those of device 1. These thinner layers form a lower ϕ_{bo2} potential barrier which is ineffective in enhancing I_{SR}. So device 2 cannot distinguish light in the visible spectrum.

The relative spectral responses of the devices were calculated at low V_{CE} bias by using parameters given in Table 1 [17]. The dark current I_{nd2}^L was obtained by putting $\Delta\phi_t^L = 0$ in eqn. 1*d*. From the formulas

$$\Phi_l = \int_0^{d_4} \Phi(x)\,dx + \int_{d_3+d_4}^{d-d_1} \Phi(x)\,dx$$

where $\Phi(x) = \eta_i \alpha(1 - R)P_i e^{-\alpha x}/hv$, the photogenerated hole current $A\Phi_l$ was obtained. The internal quantum efficiency η_i was obtained by measuring the photocurrent of an Al/p-i-n (*a*-Si : H)/ITO/glass diode. The glass side of the diode is illuminated with monochromatic light. The thicknesses of the n-, i, and p-layers of this p-i-n diode were 20, 300, and 20 nm, respectively. The reflection coefficient R of the illuminated surface is approximtely equal to 0.2 for wavelength ranging from 400 to 700 nm. The photocurrent was calculated from eqns. 1*d* and 3*b*. The calculated relative spectral responses, although not fitting well, are quite in accordance with the experimental results. A more detailed model could be needed. Furthermore, from a comparison of experimental and calculated results for device 2 which has different layer thicknesses, it was seen that the elementary model described could explain the essential features of the experimentally observed spectral responses.

Fig. 9 shows a more detailed illustration of the wavelength selectivity for device 1 at low applied V_{CE} bias. Both experimental data and the calculated results based on eqns. 1*d* and 3*b* are shown in the Figure. The experimental data reveal the peak wavelength shifts from 550 to 400 nm when the bias voltage increases from 0 to 5 V. However, the calculated results indicate a shift from 560 to 510 nm. The corresponding FWHM increases from 58 to 160 nm for the experimental data and increases from 50 to 130 nm for the calculated results. As the applied V_{CE} bias increases to a value slightly greater than 3 V, where the approach of high V_{CE} bias (eqns. 1*b* and 3*a*) is still unsuitable, the deviations of these two results being primarily due to the applicability of eqns. 1*d* and 3*b* is questionable in this voltage range. From the experimental results of other devices having layer thicknesses close those of device 1, we also found similar characteristics of wavelength selectivity. This reveals the reproducibility of the proposed device.

5 Conclusion

A new narrow-bandwidth *a*-Si : H photodetector has been demonstrated. Table 2 gives comparisons of experimental results for this device and those amorphous photodetectors reported to have voltage-selectable peak wavelength. The advantages of this photodetector include the fact that the peak wavelength can be adjusted by varying the unipolar applied bias, the lack of evident subpeak in the spectral responses, and a minimum FWHM of 58 nm at $V_{CE} = 0$ V.

Table 2: Comparisons of experimental results for proposed device and other amorphous photodetectors reported to have wavelength selectivity

Sample	1	Ref. 7	Ref. 9	Ref. 10
FWHM (nm)	58 ~ 160	>140	>100	>100
Optical gain	≤2.7	≤40	<0.4	<0.5
Peak spectral range (nm)	400~540	400~630	480~575	420~630
Adjusting voltage range (V)	0~5	0~14	−2~2	−1.5~2
Subpeak	low	low	high	low

6 References

1 TAWADA, Y., OKAMOTO, H., and HAMAKAWA, Y.: '*a*-SiC : H/*a*-Si : H heterojunction solar cell having more than 7.1% conversion efficiency', *Appl. Phys. Lett.*, 1981, **39**, pp. 237–239

2 HAMAKAWA, Y., FUJIMOTO, K., OKUDA, K., KASHIMA, Y., NONOMURA, S., and OKAMOTO, H.: 'New type of high efficiency solar cells based on *a*-Si', *Appl. Phys. Lett.*, 1983, **43**, pp. 644–646

3 SHIMIZU, I., KOMATSU, T., SAITO, K., and INOUE, E.: 'a-Si : H thin film as a photoreceptor for electrography', *J. Non-Cryst. Solids*, 1980, 35/36, p. 773
4 IMAMURA, Y., ATAKA, S., TAKASAKI, Y., KUSANO, C., HIRAI, T., and MARUYAMA, E.: 'Photoconductive imagining using hydrogenated amorphous silicon film', *Appl. Phys. Lett.*, 1979, **35**, pp. 349–351
5 MUTSUMURA, M., HAYAMA, H., NARA, Y., and ISHIBASHI, K.: 'Amorphous silicon image sensor IC', *IEEE Electron Device Lett.*, 1980, **EDL-1**, p. 182
6 CHANG, C.Y., CHANG, K.C., FANG, Y.K., and JWO, S.C.: 'The heterojunction amorphous n^+(*a*-Si)/n-i-p(*a*-SiC)/i-n^+(*a*-Si) phototransistor with high gain ($\sim$40) and high speed ($\sim 10\ \mu s$)'. IEDM technical Digest, 1986, pp. 200–204
7 CHANG, K.C., CHANG, C.Y., FANG, Y.K., and JWO, S.C.: 'The amorphous Si/SiC heterojunction color-sensitive phototransistors', *IEEE Electron Device Lett.*, 1987, **EDL-8**, pp. 64–65
8 TSAI, H.K., LEE, S.C., and LIN, W.L.: 'Amorphous SiC/Si two-colour detector', *IEEE Electron Device Lett.*, 1987, **EDL-8**, pp. 365–367
9 TSAI, H.K., and LEE, S.C.: 'Amorphous SiC/Si three-color detector', *Appl. Phys. Lett.*, 1988, **52**, pp. 275–277
10 FANG, Y.K., HWANG, S.B., CHEN, Y.W., and KUO, L.C.: 'A vertical-type *a*-Si : H back-to-back Schottky diode for high-speed color image sensor', *IEEE Electron Device Lett.*, 1991, **EDL-12**, pp. 172–174
11 WU, B.S., CHANG, C.Y., FANG, Y.K., and LEE, R.H.: 'Amorphous silicon phototransistor on a glass substrate', *IEEE Trans. Electron Devices*, 1985, **ED-32**, pp. 2192–2196
12 CHANG, C.Y.: 'Photogeneration and recombination in a bulk barrier phototransistor', *IEEE Trans. Electron Devices*, 1986, **ED-33**, pp. 1829–1830
13 CHEN, C.Y.: 'Theory of a modulated barrier photodiode', *Appl. Phys. Lett.*, 1981, **39**, pp. 979–981
14 HONG, J.W., SHIN, N.F., WU, Y.F., JEN, T.S., and CHANG, C.Y.: 'Characteristics and analysis of the *a*-Si : H color-sensitive photodetectors'. Proceedings of Japan IEMT, 1991, pp. 101–104
15 CHANG, C.Y., WU, B.S., FANG, Y.K., and LEE, R.H. 'Amorphous silicon bulk barrier phototransistor with Schottky barrier emitter', *Appl. Phys. Lett.*, 1985, **47**, pp. 49–51
16 WOLF, M.: 'Drift fields in the photovoltaic solar energy converter cells', *Proc. IEEE*, 1963, **51**, pp. 647–693
17 HOVEL, H.J.: 'Solar cells'. Thomas J. Watson Research Center, IBM Corporation, 1975